Determination of Statherin N-Terminal Peptide Conformation on Hydroxyapatite Crystals

Wendy J. Shaw,[‡] Joanna R. Long,[†] John L. Dindot,[‡] Allison A. Campbell,[§] Patrick S. Stayton,*[,†] and Gary P. Drobny*[,‡]

Contribution from the Department of Bioengineering and Department of Chemistry, University of Washington, Seattle, Washington 98195, and Pacific Northwest National Laboratory, Richland, Washington 99352

Received December 10, 1998. Revised Manuscript Received November 22, 1999

Abstract: Proteins play an important role in inorganic crystal engineering during the development and growth of hard tissues such as bone and teeth. Although many of these proteins have been studied in the liquid state, there is little direct information describing molecular recognition at the protein−crystal interface. Here we have used ^{13}C solid-state NMR (SSNMR) techniques to investigate the conformation of an N-terminal peptide of salivary statherin both free and adsorbed on hydroxyapatite (HAP) crystals. The torsion angle φ was determined at three positions along the backbone of the phosphorylated N-terminal 15 amino acid peptide fragment (D***pSpS***SEEK***FL***RR***IG***RFG) by measuring distances between the backbone carbonyls carbons in the indicated adjacent amino acids using dipolar recoupling with a windowless sequence (DRAWS). Global secondary structure was determined by measuring the dipolar coupling between the ^{13}C backbone carbonyl and the backbone ^{15}N in the $i \rightarrow i + 4$ residues (DpSpSEEKF***L***RRI***G***RFG) using rotational echo double resonance (REDOR). Peptides singly labeled at amino acids pS_3, L_8, and G_{12} were used for relaxation and line width measurements. The peptides adsorbed to the HAP surface have an average φ of −85° at the N-terminus (pSpS), −60° in the middle (FL) and −73° near the C-terminus (IG). The average φ angle measured at the pSpS position and the observed high conformational dispersion suggest a random coil conformation at this position. However, the FL position displays an average φ that indicates significant α-helical content, and the long time points in the DRAWS experiment fit best to a relatively narrow distribution of φ that falls within the protein data bank α-helical conformational space. REDOR measurements confirm the presence of helical content, where the distance across the LG hydrogen bond of the adsorbed peptide has been found to be 5.0 Å. The φ angle measured at the IG position falls at the upper end of the protein data bank α-helical distribution, with a best fit to a relatively broad φ distribution that is consistent with a distribution of α-helix and more extended backbone conformation. These results thus support a structural model where the N-terminus is disordered, potentially to maximize interactions between the HAP surface and the negatively charged side chains found in this region, the middle portion is largely α-helical, and the C-terminus has a more extended conformation (or a mixture of helix and extended conformations).

Introduction

Protein−biomineral molecular recognition processes play an important role in hard tissue development and maintenance. These interactions are also important to the biomaterials community where osteogenic proteins and peptides may play a role in enhancing orthopedic and dental material biocompatibility.[1,2] Proteins controlling calcium phosphate mineralization include osteocalcin, osteonectin, bone sialoprotein, and osteopontin from bone tissues and the proline-rich acidic proteins and statherin found in salivary fluids.[3] Similarly remarkable crystal engineering properties have been documented in marine organisms, where soluble proteins have been shown to control crystal phase switching and to regulate the growth of specific crystal faces.[4] Several models have been proposed for protein and peptide recognition of biomineral surfaces. The lattice-matching model emphasizes specific interactions of side chains with a surface site or ion, for example, the side-chain carboxylate

* Authors to whom correspondence may be sent. Gary Drobny, Department of Chemistry Box 351700, University of Washington, Seattle, WA 98195. Telephone: (206) 685-2052. Fax: (206) 685−8665. E-mail: drobny@chem.washington.edu. Patrick S. Stayton, Department of Bioengineering, Box 352125, University of Washington, WA 98195. Telephone: (206) 685-8148. Fax: (206) 685-8256. E-mail: stayton@u.washington.edu.

[†] Department of Bioengineering, University of Washington.

[‡] Department of Chemistry, University of Washington.

[§] Pacific Northwest National Laboratory.

(1) Raj, P. A.; Johnsson, M.; Levine, M. J.; Nancollas, G. H. *J. Biol. Chem.* **1992**, *267*, 5968.

(2) Weiner, S.; Addadi, L. *J. Mater. Chem.* **1997**, *7*, 689.

(3) (a) Stupp, S. I.; Braun, P. V. *Science* **1997**, *277*, 1242−8. (b) George, A.; Sabsay, B.; Simonian, P. A.; Veis, A. *J. Biol. Chem.* **1993**, *268*, 12624−30. (c) Goldberg, H. A.; Warner, K. J.; Stillman, M. J.; Hunter, G. K. *Connect. Tissue. Res.* **1996**, *35*, 385−92. (d) Hunter, G. K.; Hauschka, P. V.; Poole, A. R.; Rosenberg, L. C.; Goldberg, H. A. *Biochem. J.* **1996**, *317*, 59−64. (e) Hunter, G. K.; Goldberg, H. A. *Biochem. J.* **1994**, *302*, 175−9. (f) Kestell, M. F.; et al. *Hepatology* **16**, 1315−21 1992. (g) Fujisawa, R.; Wada, Y.; Nodasaka, Y.; Kuboki, Y. *Biochim. Biophys. Acta* **1996**, *1292*, 53−60.

(4) (a) Johnsson, M.; Levine, M. J.; Nancollas, G. H. *Crit. Rev. Oral Biol. Med.* **1993**, *4*, 371. (b) Aizenberg, J.; Hanson, J.; Koetzle, T. F.; Weiner, S.; Addadi, L. *J. Am. Chem. Soc.* **1997**, *119*, 881−886. (c) Belcher, A. M.; et al. *Nature* **1996,** *381*, 56−58. (d) Berman, A.; Addadi, L.; Weiner, S. *Nature* **1988**, *331*, 546−548. (e) Berman, A.; et al. *Science* **1993**, *259*, 776−779. (f) Falini, G.; Albeck, S.; Weiner, S.; Addadi, L. *Science* **1996**, *271*, 67−69. (g) Hanein, D.; Geiger, B.; Addadi, L. *Science* **1994**, *263*, 1413−6.

10.1021/ja9842823 CCC: $19.00 © 2000 American Chemical Society
Published on Web 02/10/2000

of glutamic acid with Ca^{2+}. In this model, α-helix or β-sheet secondary structure scaffolds (which may be present in solution or induced upon adsorption to the surface) position the interacting side chains with a periodicity or registry that matches ions in the crystal lattice.[5] Electrostatic interaction theory considers the overall charge of the peptide and the interaction of that charge with the potential of the biomineral surface.[6] An amphipathic helix could be oriented with the surface in this manner. Both models have typically been based on protein structure predictions from circular dichroism of solubilized proteins or from theoretical secondary structure predictions, and thus there is a clear need for direct determination of the secondary structure of proteins and peptides adsorbed on the mineral surface.

To define the interaction mechanisms utilized by proteins to engineer biominerals, it is important to elucidate the structure of proteins and peptides on crystal surfaces. Solid-state NMR (SSNMR) has provided high-resolution structural and dynamic information of biomolecules in mesogenic or amorphous solids where X-ray crystallographic and solution NMR approaches are not applicable.[7−13] Here we have used both homonuclear and heteronuclear dipolar recoupling techniques to investigate the structure of the lyophilized N-terminal 15 amino acid peptide fragment of statherin, both free and adsorbed to HAP crystals. Statherin is a 43-residue protein[14,15] that stabilizes supersaturated saliva by inhibiting both primary and secondary HAP crystallization.[16,17] The N-terminal domain of statherin has a high affinity for calcium phosphates such as hydroxyapatite.[18] The negatively charged residues at the N-terminus, including two phosphoserines, likely mediate this interaction.[19] The N-terminal 15-residue fragment inhibits HAP crystal growth at least as strongly as the parent protein,[1] and circular dichroism suggests the soluble peptide contains some α-helical structure.[20−22] This structure has been proposed to play a role in the recognition of HAP by statherin[1,21] and has been similarly proposed for protein−crystal interactions in other biological settings.[23−26]

Dipolar recoupling with a windowless sequence (DRAWS)[27] is a homonuclear dipolar recoupling technique that can be used to measure distances between adjacent backbone carbonyl carbons in peptides and proteins. DRAWS is well suited for studying peptide systems because it suppresses the chemical shift anisotropies (CSAs) and thus allows the observation of homonuclear dipolar couplings even when they are much smaller than the CSAs of the observed nuclei, as is the case with carbonyl carbons in peptides. These distance measurements allow direct determination of a single torsion angle φ, independent of other torsion angles or any structural models. DRAWS also has the potential to distinguish conformational heterogeneity since the dipolar recoupling efficiency is independent of any correlation between the chemical shifts and the peptide structure in a given sample.[28] Experimentally, $^{13}C-^{13}C$ distances of 4 Å have been measured with DRAWS to an accuracy of 0.1 and 5.5 Å distances have been measured to an accuracy of 0.2 Å.[27,29] To study the conformation of the N-terminal fragment in detail, we have synthesized isotopically enriched peptides shown here (where ***italics*** indicate the amino acids containing the ^{13}C-enriched backbone carbonyl carbons).

SN15-pSpS D***pSpS***EEKFLRRIGRFG

SN15-FL DpSpSEEK***FL***RRIGRFG

SN15-IG DpSpSEEKFLRR***IG***RFG

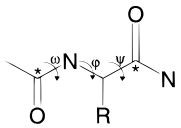

Rotation-echo double-resonance (REDOR) is a heteronuclear recoupling technique used here to measure $^{13}C-^{15}N$ distances in $i \rightarrow i + 4$ residues. This corresponds to the distance across the hydrogen bond in a helical peptide or protein.[30] This can thus be used to confirm the presence of helical structure, since the distance measured for a classical helical peptide is 4.2 Å, whereas the extended or β-sheet distance is on the order of 8−10 Å, well outside the range of this technique for these nuclei. The following peptide was prepared for determination of the global secondary structure (where the residue in ***italics*** indicates a ^{13}C-labeled backbone carbonyl and the ***underlined italics*** indicates a labeled backbone ^{15}N):

SN15-LG DpSpSEEKF***L***RRI***G***RFG

These four samples allow the determination of secondary structure at both ends as well as in the middle of the peptide (Figure 1). The carbonyl−carbonyl distances can be correlated to the torsion angle φ, and the carbonyl−nitrogen distances indicate the presence or absence of a hydrogen bond, providing insight into the secondary structure of the peptide free and adsorbed to the surface of hydroxyapatite.

Experimental Section

Materials. Protected amino acids and preloaded resins were purchased from Novabiochem (San Diego, CA) and Advanced Chemtech (Louisville, KY). Carbonyl ^{13}C-labeled serine, phenylalanine, leucine,

(5) (a) DeOliviera, D. B.; Laursen, R. A. *J. Am. Chem. Soc.* **1997**, *119*, 10627−10631. (b) Johnsson, M.; Levine, M. J.; Nancollas, G. H. *Crit. Rev. Oral Biol. Med.* **1993**, *4*, 371−8.
(6) Sicheri, f.; Yang, D. S. C. *Nature* **1995**, *375*, 427−431.
(7) Fernandez, V. L.; Reimer, J. A.; Denn, M. M. *J. Am. Chem. Soc.* **1992**, *114*, 9634−9642.
(8) Asakura, T., et al., *Biopolymers* **1997**, *41*, 193−203.
(9) Heller, J., et al., *Protein Sci.* **1996**, *5*, 1655−1661.
(10) Klug, C. A.; Burzio, L. A.; Waite, J. H.; Schaefer, J. *Arch. Biochem. Biophys.* **1996**, *333*, 221−224.
(11) Lansbury, P. T., et al., *Nat. Struct. Biol.* **1995**, *2*, 990−998.
(12) Merritt, M. E.; Christensen, A. M.; Kramer, K. J.; Hopkins, T. L.; Schaefer, J. *J. Am. Chem. Soc.* **1996**, *118*, 11278−11282.
(13) Simmons, A. H.; Michal, C. A.; Jelinski, L. W. *Science* **1996**, *271*, 84−7.
(14) Hay, D. I.; Smith, D. J.; Schluckebier, S. K.; Moreno, E. C. *J. Dent. Res.* **1984**, *63*, 857−863.
(15) Moreno, E. C.; Varughese, K.; Hay, D. I. *Calcif. Tissue Int.* **1979**, *28*, 7−16.
(16) Schwartz, S. S.; Hay, D. I.; Schluckebier, S. K. *Calcif. Tissue Int.* **1992**, *50*, 511−517.
(17) Wikiel, K.; Burke, E. M.; Perich, J. W.; Reynolds, E. C.; Nancollas, G. H. *Arch. Oral Biol.* **1994**, *39*, 715−21.
(18) Raj, P. A.; Johnsson, M.; Levine, M. J.; Nancollas, G. H. *J. Biol. Chem.* **1992**, *267*, 5968.
(19) Schlesinger, D. H.; Hay, D. I. *J. Biol. Chem.* **1977**, *252*, 1689−1695.
(20) Douglas, W. H., et al., *Biochem. Biophys. Res. Commun.* **1991**, *180*, 91−97.
(21) Gururaja, T. L.; Levine, M. J. *Pept. Res.* **1996**, *9*, 283−289.
(22) Naganagowda, G. A.; Gururaja, T. L.; Levine, M. *J. Biomol. Struct. Dyn.* **1998**, *16*, 91−107.
(23) Sicheri, F.; Yang, D. S. C. *Nature* **1995**, *375*, 427−431.
(24) DeOliviera, D. B. *J. Am. Chem. Soc.* **1997**, *119*, 10627−10631.
(25) Hauschka, P. V.; Carr, S. A. *Biochemistry* **1982**, *21*, 2538−2547.
(26) Manuscript in progress. M. Gilbert, P. Stayton, Department of Bioengineering, University of Washington.
(27) Gregory, D. M., et al., *Chemical Physics Lett.* **1995**, *246*, 654−663.
(28) Mehta, M. A., et al., *Solid State Nucl. Magn. Reson.* **1996**, *7*, 211−228.
(29) Gregory, D. M.; Bennzinger, T.; Burkoth, T. S.; Lynn, D. G.; Meredith, S. C.; Botto, R. E. *Solid State Nucl. Magn. Reson.* **1999**, in press.
(30) Marshall, G. R.; Beusen, D. D.; Kociolek, K.; Redlinski, A. S.; Leplawy, M. T.; Pan, Y.; Schaefer, J. *J. Am. Chem. Soc.* **1990**, *112*, 963.

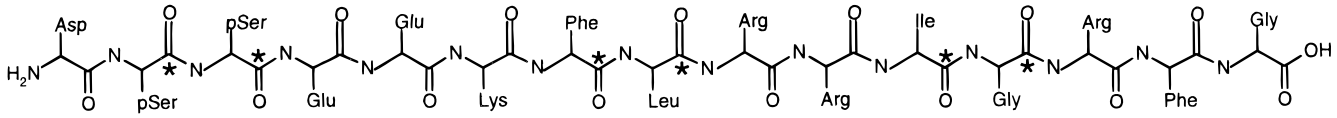

Figure 1. SN15 peptide showing the labeling scheme incorporated into three separate peptides.

isoleucine, glycine, and alanine were purchased from Cambridge Isotope Laboratories (Andover, MA).

Peptide Synthesis and Characterization. FMOC protection of labeled amino acids was accomplished using a standard procedure modified from Carpino and Han.[31] The peptides were synthesized using FastMoc[32] chemistry on an automated Applied Biosystems 433A peptide synthesizer starting with Fmoc-Gly-Wang or Fmoc-Gly-Novasyn-TGA preloaded resin (substitution 0.4 mmol/g and 0.13 mmol/g, respectively). To introduce isotopically labeled phosphoserine, the unphosphorylated peptide was synthesized with labeled serine and subsequently phosphorylated using di-*tert*-butyl-*N*,*N*-diisopropylphosphoramidite followed by oxidation with 5−6 M *tert*-butylhydroperoxide to yield the *tert*-butyl-protected phosphate moiety. In all other cases, phosphoserine was incorporated during peptide synthesis using commercially available Fmoc-Ser[PO(OBzl)OH]-OH. The peptides were cleaved from the resin and purified to homogeneity on a Waters HPLC C-18 reverse phase column using a water/acetonitrile solvent system with 0.1% TFA. Peptide fractions were lyophilized and analyzed by MALDI (matrix assisted laser desorption/ ionization) mass spectrometry to establish composition and purity.

Model Peptides. Purified ***AG***G was diluted to 10% with natural abundance AGG to control for intermolecular dipolar couplings. The peptide was then crystallized from water and analyzed using X-ray diffraction to verify a structure agreeing with published results.[33] ***FL***R was diluted to 20% with natural abundance FLR and lyophilized for study.

Hydroxyapatite (HAP) Preparation. The HAP crystals were prepared by dropwise addition of 40 mL of a solution containing 0.25 M $(NH_4)_2HPO_4$ and 2.7% NH_4OH, to 0.9 L of boiling 0.20 M $Ca(NO_3)_2$ over a 3 h period. The slurry was then refluxed for an additional 15 min. The product was filtered, dried at 110 °C, and calcined at 900 °C for 24 h. HAP was characterized by X-ray powder diffraction to confirm the absence of other calcium phosphate phases. Crystal specific surface area was determined to be 17 m^2/g using N_2 BET measurements.

Phosphate Buffer. pH 7.4 phosphate buffer was prepared with the following concentrations: 100 mM NaCl, 40 mM KCl, 4.3 mM Na_2HPO_4, and 1.4 mM KH_2PO_4. This was modified from standard PBS buffer in that the K^+/Na^+ ratio was increased to minimize pH changes upon freezing.[34]

Peptide Adsorption to HAP. The phosphorylated peptides were adsorbed to HAP by adding a solution of 1.5−3 mM peptide in phosphate buffer to 100 mg of HAP crystallites (previously washed with NaOH and phosphate buffer) and adjusting to pH 7.4, as necessary. The mixture was shaken vigorously for 5 min, then allowed to equilibrate with periodic mixing. After 2 h, the HAP crystallites were separated from the peptide in solution via centrifugation and washed repeatedly with buffer solution. The supernatant containing the unbound peptide was then frozen with liquid nitrogen and lyophilized for study. The peptide adsorbed to HAP was also frozen and lyophilized in preparation for SSNMR experiments.

SSNMR Studies. Chemical shift spectra were taken using cross polarization with magic angle spinning (CPMAS) on a home-built spectrometer operating at a ^{13}C frequency of 125.74 MHz using a home-built, triply resonant MAS probe. These experiments employed a ^1H 90° pulse width of 5 μs followed by a contact time of 2 ms and a spinning speed of 5000 Hz; 512 scans were taken for the samples off the surface. The samples on the surface were signal-averaged for 5120 scans (SN15-FL) or 10240 scans (SN15-IG and SN15-pSpS). The chemical shifts were referenced externally to crystalline 1,4-^{13}C succinic acid and converted to a tetramethylsilane reference by the addition of 180.8 ppm.

DRAWS experiments were carried out on a home-built spectrometer operating at a ^{13}C NMR frequency of 100.7 MHz using a Doty Scientific triply resonant magic angle spinning probe. Cross polarization was generated with a 5 μs ^1H 90° pulse followed by a 2 ms mixing time. The DRAWS pulse sequence consists of a windowless pulse train applied in synchrony with the rotor cycle.[27] The transverse magnetization is then observed stroboscopically every four rotor cycles and normalized with respect to the magnetization observed without any DRAWS dephasing. A ^{13}C rf field of either 38.5 kHz or 37.3 kHz, corresponding to a 6.5 μsec or 6.7 μs $\pi/2$ pulse, respectively, was used during the DRAWS mixing period, with proton decoupling of >110 kHz applied throughout the DRAWS and acquisition periods. The samples were spun at 4525 ± 5 Hz or 4390 ± 5 Hz to match with the 221 μs or 227.8 μs DRAWS cycle time, respectively. Each DRAWS experiment was run at least three times, using either 512 or 2048 scans per spectrum and a repetition time of 4 s. Adsorbed samples consisted of approximately 8−10 mg of phosphopeptide adsorbed to 100 mg of HAP packed into a 5 mm rotor. The DRAWS data were obtained on three doubly labeled SN15 samples containing differing isotopic labels. Simulated DRAWS decay curves were calculated using numerical methods that incorporated the observed relaxation times from singly labeled peptides, chemical shift anisotropies, and experimental parameters.

REDOR experiments utilized a Chemagnetics spectrometer operating at 300 MHz proton frequency. A triply resonant Chemagnetics probe was used, with a ^{13}C rf field of 43 kHz (11.6 μs π pulse), an ^{15}N field of 45 kHz (11.1 μs π pulse), and a decoupling field of 70 kHz throughout, at a spinning speed of 4 kHz. XY8 phase cycling was used on both channels to minimize pulse imperfections and offset effects, with the dephasing pulses on the $^1/_2$ rotor period and the observe pulses on the rotor period. For the peptide off the surface 1024 scans were taken, and for the adsorbed peptide, 2560 scans were taken every 8 rotor cycles, out to 104 rotor periods for both samples. Simulated REDOR decay curves were calculated using numerical methods that incorporated chemical shift anisotropies and experimental parameters.

Analysis of Conformational Distributions. Simulated DRAWS dephasing curves representing Gaussian distributions were generated by summing simulations using an increment of 0.5 standard deviations (σ) and weighting them according to their Gaussian probabilities out to 3 standard deviations (3σ). For each set of experimental data, a χ^2 analysis was performed for a series of distributions about the average value determined by the first 5−8 ms of dephasing. The single conformation, Gaussian distribution models with standard deviations of ± 10°, ± 20°, ± 30°, and an average distribution of ± 50° were analyzed. The latter distribution was used, rather than a Gaussian distribution with a standard deviation of ± 50°, which better reflects the inherent torsional constraints of the peptide bond. Last, weighted distributions representing φ angle populations observed in random coil, α-helix or 3_{10} helix protein secondary structures were simulated. These weighted distributions are based on the observed torsion angles in secondary structures of 85 proteins, yielding distributions that are more representative of the torsion angles that are typically sampled for given secondary structures.[37]

The reduced χ^2 (χ_v^2) values in Tables 2 and 3 were generated using the following equations:[35,36]

(31) Carpino, L. A.; Han, G. Y. *J. Org. Chem.* **1972**, *37*, 3404.

(32) (a) *Peptide Synthesizer User's Manual*; Applied Biosystems Inc., 1993, Vol. 433A, pp 3−15. (b) Fields, C. G.; Lloyd, D. H.; Macdonald, R. L.; Ottesen, K. M.; Noble, R. L. *Pept. Res.* **1990**, *4*, 95−101.

(33) Lalitha V.; Subramanian E.; Bordner J. *Ind. J. Pure Appl. Phys.* **1985**, *23*, 506.

(34) van den Berg, L.; Rose, D. *Arch. Biochem. Biophys.* **1959**, *81*, 349.

(35) Bevington, P. R.; Robinson, D. K. *Data Reduction and Error Analysis for the Physical Sciences;* WCB/McGraw-Hill: Boston, 1992.

(36) Gebe, J. A.; Allison, S. A.; Clendenning, J. B.; Schurr, J. M. *Biophys. J.* **1995**, *68*, 619−633.

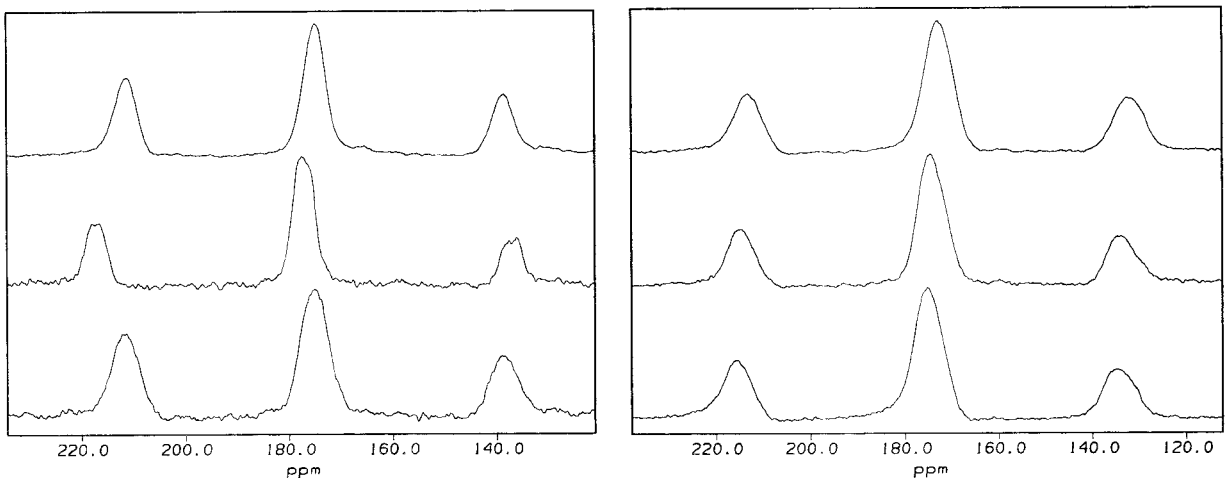

Figure 2. ^{13}C CPMAS spectra of peptides lyophilized (left) and adsorbed to hydroxyapatite (right). From top to bottom: SN15-pSpS, SN15-FL, and SN15-IG.

$$\chi^2 = \sum_i \frac{(E_i - S_i)^2}{\sigma^2} \quad (1)$$

where E_i is the experimental value for data point i, S_i is the simulated value for data point i, σ is the standard deviation of the experimental data, and

$$\chi_v^2 = \frac{\chi^2}{\nu} \quad (2)$$

where ν is the number of degrees of freedom. The relative probabilities were calculated using

$$\frac{P_1}{P_2} = \exp[-(\chi_1^2 - \chi_2^2)/2] \quad (3)$$

where χ_1^2 is calculated for the simulation of a single conformation and χ_2^2 corresponds to the simulation of a given distribution. Therefore, a relative probability less than one ($P_2 > P_1$) indicates the experimental data is best described by the simulated distribution rather than a single conformation, and a relative probability greater than 1 ($P_2 < P_1$) indicates that a single conformation best describes the data. A relative probability between 0.51 and 1.95 (within a standard deviation) indicates the difference between the two simulations is statistically insignificant.

Results

Peptide Characterization. Peptides were purified to homogeneity using reverse-phase HPLC. MALDI mass spectrometry analysis of the purified peptide yielded molecular weights of 1959.2 (SN15-pSpS), 1959.8 (SN15-FL), 1959.6 (SN15-IG), 1959.9 (SN15-pS$_3$), 1958.7 (SN15-L$_8$), and 1959.0 (SN15-G$_{12}$) Da (theoretical MW: 1959.8 Da).

Chemical Shift Characterization. The CPMAS spectra of lyophilized and adsorbed peptides are shown in Figure 2. The isotropic chemical shift values and line widths for each of the singly and doubly labeled SN15 peptides on and off the HAP crystal surface are given in Table 1. SN15-pSpS displays two overlapping peaks convoluted into one broad resonance both on and off the surface (total line width 7.16 and 5.18 ppm, respectively). SN15-FL off the surface displays two overlapping resonances (combined peak width 5.06 ppm) in the CPMAS spectrum. When adsorbed to the surface, SN15-FL displays a combined line width of 7.07 ppm. SN15-IG displays two unresolved resonances (total line width 5.4 ppm) off the surface, which remain unresolved when adsorbed to the surface (total peak width 7.05 ppm). Singly labeled peptides have line widths off the surface of 4.2 ppm (SN15-pS$_2$), 3.3 ppm (SN15-pS$_3$), 3.9 ppm (SN15-F$_7$), 3.4 ppm (SN15-L$_8$), 3.6 ppm (SN15-I$_{11}$), and 5.3 ppm (SN15-G$_{12}$). On the surface, the line widths are 7.3 ppm (SN15-pS$_2$), 6.0 ppm (SN15-pS$_3$), 6.6 ppm (SN15-F$_7$), 6.6 ppm (SN15-L$_8$), 6.9 ppm (SN15-I$_{11}$), and 6.8 ppm (SN15-G$_{12}$).

Table 1. Chemical Shift Values and Linewidths of SN15 as a Lyophilized Free Peptide and Adsorbed on the Surface of HAP

	chemical shift off/on surface (ppm)	double labels line width off/on surface (ppm)	single labels line width off surface (ppm)	single labels line width on surface (ppm)
SN15-pSpS	173.0/ 172.4	5.18, 7.16	4.2, 3.3	7.3, 6.0
SN15-FL	175.6/ 174.5	5.06, 7.07	3.9, 3.4	6.6, 6.6
SN15-IG	175.1/ 175.0	5.4, 7.05	4.17, 5.27	6.96, 6.81

DRAWS Measurements. To test the ability of DRAWS data to identify structural dispersions, DRAWS data were obtained for the crystalline tripeptide ***AG***G, and for the lyophilized peptide, ***FL***R. Figure 3a shows the experimental DRAWS dephasing curve of ***AG***G, a doubly carbonyl-labeled crystalline peptide, along with simulations for $\varphi = -73°$, $-83°$, and $-93°$. Additionally, a simulation (dotted line) for an average φ of $-83°$ with Gaussian distribution of conformations ($\sigma = 30°$) is shown. Inspection of Figure 3a shows that the $\varphi = -83°$ simulation fits the data better than $\varphi = -73°$ or $\varphi = -93°$. Table 3 compares the change in χ^2 observed when comparing the first 6 points of the two curves versus comparing all 21 points. For the crystalline peptide (***AG***G) the change in χ^2 comparing the single conformation to a distribution for the first 6 points is very small (2.96×10^4) in comparison to the relative probability observed when the entire curve is taken into consideration (5.08×10^{49}). For the lyophilized, noncrystalline ***FL***R tripeptide (Figure 3b), the early timepoints are best fit using $\varphi = -103°$. A Gaussian distribution of structures ($\sigma = 30°$) fits the data with a higher relative probability (9.18×10^{-6}) than a single conformation (Table 3) (the large negative rather than positive exponent resulting from the definition of P_1/P_2).

The DRAWS dephasing curves for SN15-pSpS on and off HAP are shown in Figure 4. The bars represent the standard deviation in multiple distance measurements made on the same sample. The average distances obtained from the first 7−10 points in the dephasing curve are shown in Table 2. SN15-pSpS on the surface of HAP displayed an average $\varphi = -85°$ (3.18 Å), and a confidence level (based on χ_v^2 and taken from standard tables[35]) of 95−98%. The accuracy of DRAWS at these

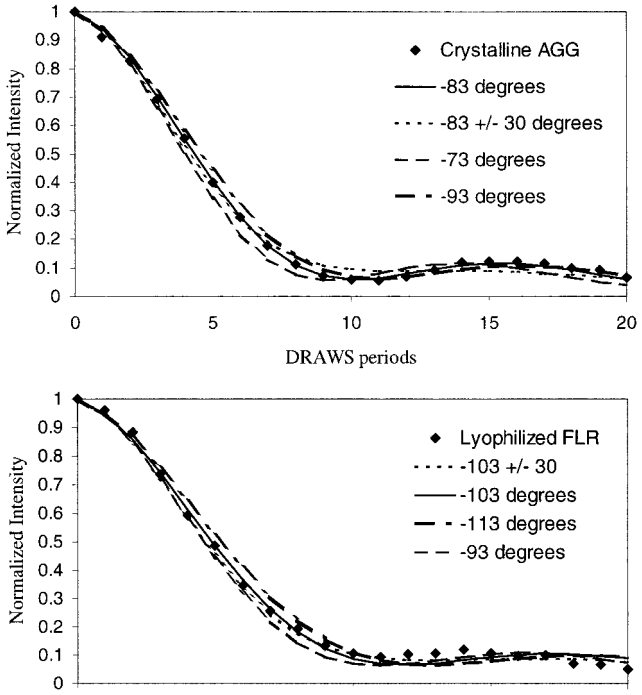

Figure 3. These two peptides illustrate the ability of DRAWS to indicate structural heterogeneity. The upper graph is for an ordered, crystalline tripeptide, ***AG***G. The experimental data is represented by diamonds, and the simulation for the crystallographic torsion angle φ of $-83°$ is a solid line. The dashed line is a simulation using an average φ angle $-83°$ with a Gaussian distribution of $\pm 30°$. Visually, the single conformation is a much better simulation of the experimental data. This is also supported statistically in Table 3, where the single conformation has a 5.08×10^{49} higher relative probability based on χ-squared to fit the data then the Gaussian distribution. The lower graph shows data and simulations for a disordered tripeptide, ***FL***R. The solid line represents a single conformation of $-103°$; the dashed line a Gaussian distribution of $-103° \pm 30°$. In Table 3, it is shown that the distribution fits the data with a 9.18×10^{-6} higher relative probability than the single conformation. In both cases it is important to note that applying a distribution only marginally changes the average distance.

Table 2. φ Determined at the Three Labeled Sites in SN15 and the χ_v^2 of the First 7−10 Points in the DRAWS Dephasing Curve. the Probabilities Obtained from Standard Tables[35] Are Shown as Percentages in Parentheses

	average φ (deg)	χ_v^2 (confidence level)
SN15-pSpS off HAP	−85	0.348 (90−95%)
SN15-pSpS on HAP	−85	0.271 (95−98%)
SN15−FL off HAP	−73	0.215 (99%)
SN15−FL on HAP	−60	0.391 (85−90%)
SN15−IG off HAP	−80	0.183 (99%)
SN15−IG on HAP	−73	0.218 (95−98%)

distances is generally within 0.1 Å ($\varphi = \pm 10°$) when using two-spin simulations.[27] Statistical analysis of the longer time points indicates that for the pSpS region of SN15 on the surface, the DRAWS data is best fit with a random coil distribution of φ (relative probability $= 1.41 \times 10^{-7}$ from eq 3). DRAWS dephasing curves of SN15-pSpS off the surface fit an average φ of $-85°$ (3.18 Å) with a confidence level of 90−95%. The longer data points for SN15-pSpS off the surface are modeled most accurately by applying a $\pm 20°$ Gaussian distribution of conformations (relative probability $= 0.091$).

SN15-FL on the surface yields a shorter distance of 2.98 Å, corresponding to a φ of $-60°$, at a confidence level of 85−90%. For the peptide on the surface, models of a single conformation or small distributions of $\leq 20°$ fit the long time points equally well. SN15-FL displayed an average distance of 3.09 Å off the surface corresponding to $\varphi = -73°$ at the 99% confidence limit (Figure 5). The longer time points are modeled well with a distribution of $\pm 20°$, or by a weighted distribution of angles observed for 3_{10} helices.[37]

The average distance of SN15-IG adsorbed to HAP is 3.08 Å ($\varphi = -73°$, confidence level 95−98%) with the later data points indicating a larger Gaussian distribution of $\pm$ 30° to $\pm$ 50° or a random coil distribution.[37] The average distance of SN15-IG measured off the surface was 3.14 Å, corresponding to a φ torsion angle of $-80°$ (confidence level 95−98%), with a distribution being best described by a single conformation or by Gaussian distributions of $\pm 10°$ or $\pm 20°$ (see Figure 6).

REDOR measurements. S/S_0 REDOR curves are shown in Figure 8, where the bars on the experimental data indicate the standard deviation of multiple measurements on the same sample. Simulations of 4.0, 4.5, 5.0, and 5.5 Å are also shown. The measured distance of SN15-LG off the surface was found to be 4.4 ± 0.3 Å. The peptide adsorbed to HAP had a slightly longer distance of 5.0 ± 0.5 Å.

Discussion

Protein structure and biomineral recognition are closely tied, and thus the determination of protein structure on crystal surfaces is an important fundamental goal. SSNMR techniques provide a unique route to determining molecular structure at the protein/inorganic solid interface. In this study, we have utilized the DRAWS technique to measure distances between adjacent backbone carbonyl carbons in N-terminal peptides of the salivary protein statherin. The distance measurement from DRAWS is independent of the angle ψ, resulting in a direct and unambiguous measurement of φ at the selected backbone positions. Three labeling schemes were used to independently probe the conformation of the 15mer: near the N-terminus, in the middle of the peptide, and near the C-terminus. For a peptide with classical ideal α-helical structure ($\varphi = -57$), a distance of 2.95 Å is expected between adjacent backbone carbonyl carbons. The distance expected for a fully extended secondary structure ($\varphi = -180$) would be 3.7 Å, and for a β sheet structure ($\varphi = -119$) would be 3.5 Å. A more recent study based on the high-resolution crystal structure of 85 proteins suggests less rigid definitions, with the α-helical structure having an average $\varphi = -65° \pm 13°$ and β sheet $\varphi = -113° \pm 41°$.[37]

The observed dephasing in the first 5−8 ms of the DRAWS experiment is determined by the average dipolar coupling or distance and is largely independent of conformational dispersion, while the long timepoints in the dephasing curve contain information on conformational dispersion.[28] The question of conformational distribution is an important aspect of these structural determinations, and while the signal-to-noise levels at the longer time points in these DRAWS experiments are relatively low, we have conducted a statistical analysis of the data in order to determine the statistical significance of simulations that include conformational dispersion. The ability of DRAWS to distinguish conformational distributions is demonstrated in the experimental DRAWS dephasing curves

(37) Smith, L. J.; Bolin, K. A.; Schwalbe, H. MacArthur, M. W.; Thornton, J. M.; Dobson, C. M. *J. Mol. Biol.* **1996**, *255*, 494−506.

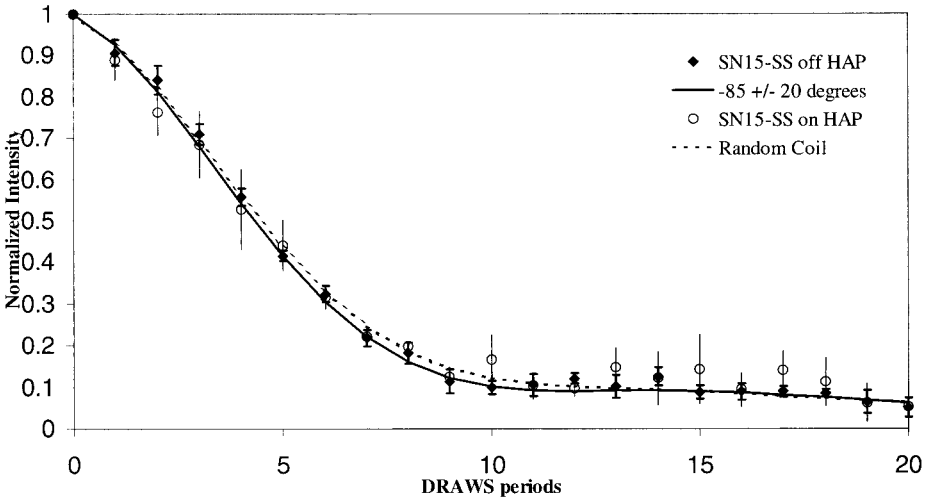

Figure 4. Experimental DRAWS dephasing curve of SN15-pSpS on HAP (open circles) and off HAP (diamonds). The average distance for SN15-pSpS on HAP is fit most accurately (solid line) by $\varphi = -85°$ (3.18 Å). The longer time points are more closely fit by a Gaussian distribution of $\sigma = 30°$ around $-85°$ (dashed line), or by a distribution commonly observed in proteins to be random coil, indicating that the peptide has little structure at the N-terminus. SN15-pSpS off of the HAP surface has similar secondary structure with slightly less conformational heterogeneity, where the best fit is $\varphi = -85°$ with a Gaussian distribution of $\pm 20°$.

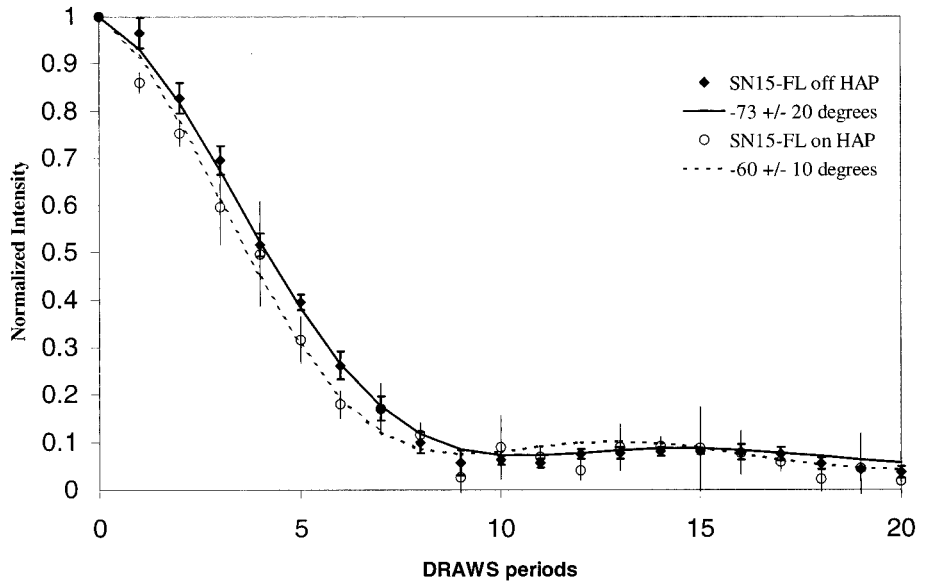

Figure 5. Experimental DRAWS dephasing curves of SN15-FL off HAP (diamonds) and SN15-FL on HAP (open circles). The simulated fit for SN15-FL off HAP (solid line) is 3.09 Å, corresponding to an average φ angle of $-73°$. At longer times, applying a distribution of $\pm 20°$ fits the data more accurately, as well as a distribution of angles seen for 3_{10} helices. The fit for SN15-FL on HAP (dashed line) is 3.0 Å, which corresponds to a φ of $-60°$. The data are fit within a standard deviation by a single conformation, a Gaussian distribution of $\pm 10°$ and a Gaussian distribution of $\pm 20°$. The average torsion angles correspond to angles commonly observed for helices.

of crystalline ***AG***G and lyophilized ***FL***R, where the improved fit to DRAWS data for ***FL***R obtained with a φ distribution of $\pm 30°$ is shown in Table 3 to be statistically significant. There are experimental parameters such as insufficient decoupling or phase transients that can result in dephasing behavior similar to that produced by a distribution.[28] Although this is an important consideration, attempts are made to remove these experimental contributions, the success of which is demonstrated in the model peptide data (Figure 3). It should be noted that the reduced χ^2 for AGG shown in Table 3 is large compared to the reduced χ^2 values for SN15 peptides (Table 2). This demonstrates that χ^2 values themselves must be interpreted with some degree of caution. The reduced χ^2 given by eq 2 is frequently interpreted as measuring the agreement between data and a model, but only does so within the uncertainties associated with the data.[35] Therefore, data with small experimental uncertainties can yield a large χ^2 because the inadequacies of the model become evident.

The average φ ($-60°$) at the FL position in the SN15 peptide falls in classical α-helical conformational space, indicating there is substantial secondary structure in the central region of SN15 when adsorbed to HAP. REDOR experiments confirm the helical structure in the middle portion of the peptide, yielding a distance of 5.0 Å, compared to the expected distance of 4.22 Å.[38] The N-terminal binding site (pSpS) displays the largest φ ($-85°$), and the longer time points in the dephasing curve are best fit by a random coil distribution model (vide infra). This is consistent with a disordered N-terminus, which may allow the negatively charged side chains and phosphates at the serine positions to interact maximally with the HAP surface. The IG

(38) Calculated using Insight II, assuming classical φ and ψ angles for the helix.

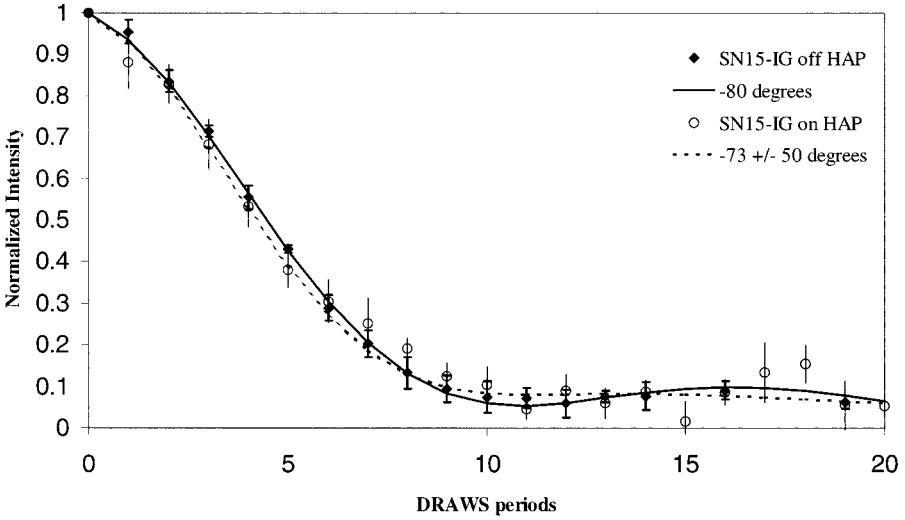

Figure 6. Experimental DRAWS dephasing curves of SN15-IG off HAP (diamonds) and SN15-IG on HAP (open circles). The simulated fit to the experimental data for SN15-IG on HAP is $\varphi = -72°$ (3.08 Å). Long time points are best fit by an average distribution of $\pm$ 50° around −72°, or by a distribution of angles observed for 3−10 helices. SN15-IG off HAP fits an average distance of 3.15 Å, corresponding to a $\varphi = -80°$. These data is fit equally well by a single conformation, or by a distribution of conformations with $\sigma = 10°$ or 20°.

Table 3. Simulations of Short Model Peptides Demonstrating the Ability of DRAWS to Simulate a Distribution without Significantly Affecting the Average Distance

	simulation (deg)	χ_v^2 for average distance	χ_v^2 for entire curve	relative probability (first 7−10 points/entire curve)
AGG-crystalline	−83	0.7511	0.9	
	−83 ± 30	4	12.4	4.07e5/5.08e49
FLR-lyophilized	−103	0.323	2.15	
	−103 ± 30	0.505	1	0.44/9.18e-6

position exhibits an average φ of −73° on the surface, which is at the upper end of α-helical space. The broad conformational dispersion observed suggests that the C-terminus exists with some distribution between α-helix and more extended structures. The large dispersion at the C terminus could be related to the lack of a hydrogen bond donor available for the glycine position due to its proximity to the C-terminus**.** The REDOR-measured distance is slightly longer than expected for a classical α-helix with no conformational heterogeneity and thus consistent with a more extended C-terminus. The confidence limits shown in Table 2 demonstrate that there is a high confidence in the average distances measured for these peptides regardless of any conformational heterogeneity which may be present. Similar φ values on and off the surface for all regions of the peptide suggest that the peptide does not exhibit a large change in structure upon binding to HAP. There is a small but significant shortening at the FL position upon adsorption that suggests binding energy might be used to stabilize α-helical structure in the middle region of the peptide. Figure 7 summarizes our data, demonstrating the best distribution model for each peptide as a function of the torsion angle φ, both off and on the surface.

The chemical shifts and line widths potentially contain complementary information to the DRAWS data, as chemical shifts have traditionally been used to qualitatively distinguish between various secondary structures.[39] Although the carbonyl-labeling scheme utilized here limits the interpretation of the absolute chemical shift, the line width of the carbonyl resonances can be indicative of conformational heterogeneity. The observed line widths for the singly labeled SN15-pS_2, SN15-pS_3, SN15-F_7, SN15-L_8, and SN15-I_{11} (3−4 ppm) off the surface are typical of lyophilized, ordered peptides, which have line widths of 2−4 ppm.[40] The line width of SN15-G_{12} is greater than 5 ppm, reflecting structural heterogeneity at the C-terminus of the free peptide. All SN15 carbonyl line widths increase 1.5−2 times upon adsorption to the surface. This increased breadth could be due to conformational heterogeneity, relaxation processes, and the anisotropic magnetic susceptibilities of the HAP crystals.[41,42] The measured T_2^{SQ} value of 12.5 ms indicates that relaxation processes are not contributing greatly to the line widths. However, the volume magnetic susceptibilities of crystalline phosphate salts are large and typically range from −150 to −200 ppm cm^3.[43] Although MAS reduces the isotropic magnetic susceptibility, the anisotropic magnetic susceptibility is not removed by MAS and may contribute to the observed line width of the adsorbed peptides.[41] Recent studies with hydrated surface adsorbed peptides[44] demonstrate that a significant portion of the observed line broadening is due to this large magnetic susceptibility. When the surface adsorbed peptide is hydrated, the singly labeled line width is reduced from 6.0 to 3.4 ppm in the case of SN15-pS_3. The chemical shift anisotropy is narrowed only slightly (approximately 10 ppm), indicating that motion is not a primary narrowing mechanism. This suggests that wetting the surface fills the spaces between the HAP crystals with buffer, partially matching the anisotropic susceptibility of the HAP particles, resulting in narrowed lines. A similar effect was reported by Elbayed et al.[42] Some conformational dispersion is certainly expected, and the hydrated line widths on the order of 3−4 ppm suggest there is some conformational dispersion contributing to the line width

(39) (a) Fuijisawa, R.; Kuboki, Y. *Eur. J. Oral Sci.* **1998**, *106*, 249−253. (b) Wishart, D. S.; Sykes, B. D. *J. Biomol. NMR* **1994**, *4*, 171. (c) Asakawa, N.; Kuroki, S.; Kurosu, J.; Ando, I.; Shoji, A.; Ozaki, T. *J. Am. Chem. Soc.* **1992**, *114*, 3261. (d) Asakawa, N.; Kurosu, H.; Ando, I. *J. Mol. Struct.* **1994**, *323*, 279.

(40) (a) Unpublished results. (b) Long, H. W.; Tycko, R. *J. Am. Chem. Soc.* **1998**, *120*, 7039.

(41) (a) VanderHart, D. L.; Earl, W. L.; Garroway, A. N. *J. Magn. Reson.* **1981**, *44*, 361−401. (b) Stoll, M. E.; Majors, T. J. *J. Magn. Reson.* **1982**, *46*, 283−288.

(42) (a) Elbayed, K.; Bourdonneau, M.; Furrer, J.; Richert, T.; Raya, J.; Hirshcinger, J.; Piotto, M. *J. Magn. Reson.* **1999**, *136*, 127−129.

(43) *Handbook of Chemistry and Physics*, 63rd ed.; Weast, R. C., Ed., CRC Press: Boca Raton, 1982.

(44) Shaw, W. J.; Long, J. R.; Campbell, A. A.; Stayton, P. S.; Drobny, G. P., manuscript submitted.

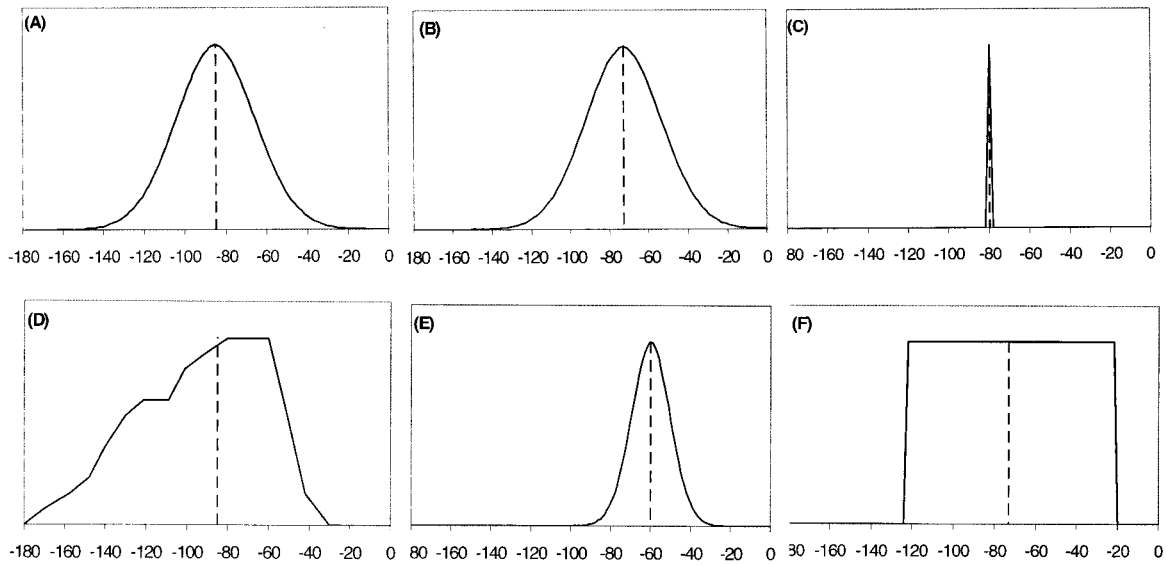

Figure 7. The distribution most closely simulating the experimental DRAWS dephasing curves are shown for each sample on and off the surface. (A) SN15-SS off HAP ($\varphi = -85 \pm 20°$), (B) SN15-FL off HAP ($\varphi = -73 \pm 20°$), (C) SN15-IG off HAP ($\varphi = -80$), (D) SN15-SS on HAP ($\varphi = -85$, with a random coil distribution), (E) SN15-FL on HAP($\varphi = -60 \pm 20°$), and (F) SN15-IG on HAP ($\varphi = -73 \pm 50°$).

as well. The chemical shifts are thus consistent with a relatively narrow but real distribution of conformations. However, given the susceptibility contributions it is difficult to use chemical shift spectra alone to assess structural heterogeneity. In contrast, DRAWS decay curves are obtained by integration of the CPMAS spectrum observed following DRAWS irradiation. Therefore DRAWS data are not perturbed by magnetic susceptibility broadening and may provide a more straightforward basis for estimating the structural dispersion of peptides adsorbed to HAP crystals.

Conclusions

We have previously determined that the N-terminal N6 statherin peptide is disordered on HAP[45] and show here that the corresponding residues remain largely unstructured in the longer peptide. The middle and C-terminal portion of the peptide on the surface exhibit conformations consistent with torsion angles expected for α-helices and a mixture of α-helices and extended structure, respectively, with REDOR data supporting a helical structure from the middle to the C-terminus (Figure 8). Electrostatic interaction theory has been implicated in the literature as a model for the interactions of peptides with the overall charge of a crystal.[1,5] The lack of a specific secondary structure observed at the pSpS position allows multiple side-chain electrostatic interactions with the surface, consistent with the fact that the phosphoserines have been shown to play a key role in binding affinity.[19] The α-helix motif has been considered to be a lattice matching conformation for side chain interactions with specific calcium ions in the HAP crystal.[6] The presence of some α-helical content in the middle and at the C-terminus of SN15 on the HAP surface is consistent with this model. Currently, we are studying the interactions of the side chains with the surface in order to determine the precise nature of binding. Additionally, we are studying SN15 and full statherin on HAP in a hydrated, buffered state to more accurately simulate the biological environment and determine the roles of structure and dynamics in regulating mineralization.

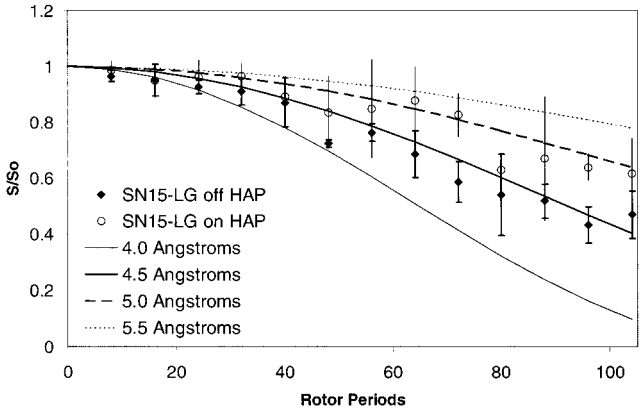

Figure 8. Experimental REDOR data of SN15-LG both on (open circles) and off (dark diamonds) HAP. The off-the-surface data fits best to a distance of 4.5 Å and the on-the-surface data fits to 5.0 Å most accurately. The expected distance for a classical α-helix is 4.22 Å, clearly indicating a significant portion of helical content both on and off the surface. Simulations shown are of 4.0, 4.5, 5.0, and 5.5 Å as indicated.

Acknowledgment. We gratefully acknowledge contributions from co-workers for CD characterization (Michele Gilbert), preparing hydroxyapatite (Lin Song), and writing simulation code (Nathan Oyler). In addition, we are most appreciative of the use of Jim Franz's 300 MHz instrument, at Battelle, PNNL. We also acknowledge the support of the National Institute of Dental Research (DE 12554-01), the National Science Foundation (EEC-9529161 and DMR-9616212), the Department of Energy (DE-AC06-76RL0 1830), and the Office of Science, Office of Basic Energy Sciences, Department of Energy, through Associated Western Universities (W.J.S.).

JA9842823

(45) Long, J. R.; Dindot, J. L.; Zebroski, H.; Kiihne, S.; Clark, R. H.; Campbell, A. A.; Stayton, P. S.; Drobny, G. P. *Proc. Natl. Acad. Sci. U.S.A.* **1998**, *95*, 12083−12087.